Numerical Study of a Journal Bearing with Scratches: Validation with Literature and Comparison with Experimental Data

Anh T Vo, Michel Fillon, Jean Bouyer

lubricants

MDPI

Article

Numerical Study of a Journal Bearing with Scratches: Validation with Literature and Comparison with Experimental Data

Anh T. Vo [1,2], Michel Fillon [1] and Jean Bouyer [1,*]

[1] GMSC Department, Pprime Institute, CNRS-University of Poitiers-ISAE ENSMA, 11 Bd Marie et Pierre Curie, TSA 41123, CEDEX 9, 86073 Poitiers, France; vtanh@dut.udn.vn (A.T.V.); michel.fillon@univ-poitiers.fr (M.F.)
[2] Department of Mechanical Engineering, University of Science and Technology, The University of Danang, 54 Nguyen Luong Bang, Danang 550000, Vietnam
* Correspondence: jean.bouyer@univ-poitiers.fr

Abstract: The lifespan of journal bearings is directly related to the operating conditions they have to face and reducing their maintenance intervals allows one to have a clear idea about their performance when issues occur. The presence of scratches on one of its surfaces degrades the performance of a journal bearing. These effects have already been assessed in experiments; however, numerical studies on this subject are still scarce. This work develops a numerical thermohydrodynamic (THD) program using the finite volume method to simulate the effects of scratches on the performance of journal bearings. To test the validity of the program, the numerical results are compared with the scientific literature and with experimental measurements conducted using the Pprime Institute journal bearing test rig. Some minor discrepancies are observed, but the overall results are in good agreement.

Keywords: surface scratches; journal bearing; thermohydrodynamic simulations; experiments

Citation: Vo, A.T.; Fillon, M.; Bouyer, J. Numerical Study of a Journal Bearing with Scratches: Validation with Literature and Comparison with Experimental Data. *Lubricants* **2021**, *9*, 61. https://doi.org/10.3390/lubricants9060061

Received: 30 April 2021
Accepted: 31 May 2021
Published: 5 June 2021

1. Introduction

Hydrodynamic journal bearings are important machine elements and one of the most common types of hydrodynamic bearings, mainly used to support high-speed rotating machinery, including turbines and compressors, pumps and motors, etc., because of their very long lifetime, high load-carrying capacity, and efficiency. Well-designed journal bearings can operate efficiently for years with minimum maintenance. However, when suffering damages or failures, the consequences can be catastrophic and lead to the damage of the machine or the interruption of plant operations.

After some time of operation, especially in severe conditions, hydrodynamic bearings are often degraded because of the presence of damage such as the loss of babbitt material, babbitt surface displacement and supporting structure degradation. This causes a loss of load capacity, significantly reducing the oil film thickness because of the decrease in the active surface area. The loss of babbitt material can be categorized using several types and names, such as bulk loss, wear, and scratches, based on the location and volume of the loss [1]. A scratch is a major type of surface damage in babbitted industrial bearings. A scratch has a narrow cross-section but a significant length; scratches can be shallow or deep [1]. Scratches can appear on the babbitted surface of the bush as well as on the rotating surface and as shown in [1], they result in a similar effect on the hydrodynamic film.

Scratches on journal bearings are a common issue observed during maintenance operations by users of steam turbines, pumps, motors, etc. Scratches on shafts are often caused by the presence of debris within the lubricating oil that is trapped in the babbitt. Scratches degrade the performance of journal bearings, but their effects were neglected for a long time. One of the earliest studies on this subject was in 2012, when Dobrica and Fillon [2] conducted a numerical study on performance degradation in scratched journal bearings.

They performed a parametric study, using a hydrodynamic numerical model with global thermal effects, to simulate scratched journal bearings. They evaluated several scratch parameters (depth, extent, density, etc.) and concluded that the bearing performance is poorer in the presence of a scratch. They also highlighted that the scratch depth appears to be the most influential parameter affecting the bearing performance, especially if the depth is greater than the bearing clearance. In 2016, Giraudeau et al. [3] carried out experimental measurements of local parameters such as pressure and temperature, and global parameters such as friction torque and flow rate, for a two-lobe journal bearing with one scratch. They showed that the scratch depth influences pressure and temperature, but also that the effects depend on the operating conditions (imposed load and speed). In 2018, Bouyer et al. [4] compared thermoelastohydrodynamic (TEHD) simulation results with the experimental results in Giraudeau et al.'s study. This TEHD model made a simplification for the scratch geometry by adding the scratch depth value to the lubricant film thickness instead of meshing the real geometry of the lubricant film domain. In 2020, Bouyer et al. [5] updated their work, and carried out experiments for multiple scratches on a journal bearing (two and sixteen scratches machined on the surface of the journal); they concluded that scratches induce a strong modification of the pressure field, increase both the maximum pressure and the maximum temperature, and significantly reduce the load-carrying capacity of the bearing.

Experimental measurements to assess scratched journal bearings are available; however, to our knowledge, there is as yet no valid thermohydrodynamic (THD) numerical model that is able to simulate scratched journal bearings by considering the real scratch geometry. Therefore, this study aims to develop a THD numerical program to simulate journal bearings which have one or more scratches with a fully known scratch geometry.

The first part of this paper presents the theoretical and numerical models. The second part compares the simulation results, first with the scientific literature and secondly with experimental data for several types of journal bearing. The studied configurations are one plain journal bearing without a scratch, one two-lobe journal bearing without a scratch, and one preloaded two-lobe journal bearing with scratches (one and two scratches). The last part presents our conclusions and further perspectives.

2. Theoretical Analysis and Numerical Modeling

2.1. Basic Equations

The generalized Reynolds differential equation derived from the Navier–Stokes equation for calculating the pressure distribution in the fluid film of journal bearings, with the assumption of Newtonian, incompressible flow in steady state operation, is given as follows:

$$\frac{\partial}{\partial x}\left(G\frac{\partial p}{\partial x}\right)+\frac{\partial}{\partial z}\left(G\frac{\partial p}{\partial z}\right)=\rho U\frac{\partial(J_1/J_0)}{\partial x} \quad (1)$$

where:

$$J_n=\int_0^h \frac{y^n}{\mu(x,y,z)}dy;\ G(x,z)=\rho\left[\int_0^h \frac{y^2}{\mu(x,y,z)}\,dy-\frac{{J_1}^2(x,z)}{J_0(x,z)}\right]$$

where p is the fluid pressure, U is the rotational speed of the journal, ρ is the fluid viscosity, and h is the fluid film thickness.

In the film rupture zone, where cavitation can occur, this study uses the cavitation model proposed by Bonneau et al. [6]. In their model, they assume that the lubricant in the film rupture zone comprises a portion of fluid and a portion of gas; the fluid film thickness h is then divided into a fluid portion r (named as the filling) plus a gas portion (h-r). The mass conservation equation is solved in this film rupture zone. The energy equation allows us to determine the oil film temperature as:

$$\rho C_p \left(u\frac{\partial T}{\partial x} + v\frac{\partial T}{\partial y} + w\frac{\partial T}{\partial z} \right) = K\frac{\partial^2 T}{\partial y^2} + \mu \left[\left(\frac{\partial u}{\partial y} \right)^2 + \left(\frac{\partial w}{\partial y} \right)^2 \right] \quad (2)$$

where T is the oil film temperature, K is the thermal conductivity of the oil, and u, v, and w are the fluid velocity components in the x, y, and z directions, respectively.

The heat conduction equation for calculating the temperature of the bush is presented below:

$$\frac{\partial^2 T_b}{\partial {r_b}^2} + \frac{1}{r_b}\frac{\partial T_b}{\partial {r_b}^2} + \frac{1}{{r_b}^2}\frac{\partial^2 T_b}{\partial {\theta_b}^2} + \frac{\partial^2 T_b}{\partial z^2} = 0 \quad (3)$$

where T_b is the bush temperature, r_b is the bush radius coordinate, and θ_b is the bush angular coordinate.

2.2. Boundary Conditions

The pressure boundary conditions are the following: at the leading and trailing edges of the bearing, the pressure equals the oil supply pressure; at both bearing sides, the pressure is equal to the ambient pressure P_{amb}. This ambient pressure is also taken as the reference pressure.

$$\begin{cases} p|_{x=x_{in}} = p_{sup} \\ p|_{x=x_{out}} = p_{sup} \\ p|_{z=0,\,L} = p_{amb} \end{cases} \quad (4)$$

The thermal boundary conditions depend on the bearing zone that is being considered:

- For the inlet temperature at the leading sections of each lobe:

$$T_{in}^{i} = \alpha^{i}\left(\frac{Q_{out}^{i-1}}{Q_{in}^{i}} \right) T_{out}^{i-1} + \left(\frac{Q_0}{Q_{in}^{i}} \right) T_{sup} \quad (5)$$

  where Q_{in}^{i}, T_{in}^{i} are the entering flow rate and entering temperature of lobe (i); Q_{out}^{i-1}, T_{out}^{i-1} are the recirculating flow rate and recirculating temperature of lobe (i-1), respectively; and Q_0 is the supplied flow rate. The fluid exiting at the outlet of lobe (i-1) is circulated to the lobe (i) with α^i, the recirculating coefficient of lobe (i), which represents a percentage of the recirculated hot oil; and T_{sup} is the temperature of the freshly supplied oil. The value of α depends on several factors and is outside the scope of this work. However, a few factors can be listed—the operating conditions, and the energy balance model in the groove. Under certain operating conditions, the flow rate at which hot oil exits from the previous lobe is greater than the entering flow rate of the current lobe, so there is no fresh oil supplied and the value of α is 1; otherwise, it is less than 1. The value of α also depends on the energy balance model in the groove. For example, several studies have considered backflow, reverse flow, or negative flow rate phenomena in their models (e.g., [7,8]), while others have simplified the model by neglecting these. In these circumstances, there are different choices for the value of α. In general, for journal bearings the value usually varies from 0.5 to 1 and the values may be different for each lobe.

- At the fluid/bush interfaces, the temperature is given by the heat flux continuity condition:

$$K_f \frac{\partial T}{\partial y}\Big|_{y=h} = -K_b \frac{\partial T_b}{\partial r_b}\Big|_{r_b=r_{b,inner}} \quad (6)$$

where K_f is the thermal conductivity of the fluid and K_b is the thermal conductivity of the bush.

- At the fluid/journal interface, the temperature of the journal surface can be either imposed or calculated; if it is calculated, then, due to the shaft rotation, it is considered to vary only in the axial direction, and so, for each transverse section, the following relationship applies:

$$\sum_{i=1}^{NL} \int_{x_{in}^i}^{x_{out}^i} \frac{\partial T}{\partial y}\Big|_{y=0} dx = 0 \quad (7)$$

where NL is the number of lobes of the bearing.

- At the outer surface of the bushing, a free convection hypothesis is applied:

$$K_b \frac{\partial T_b}{\partial r_b}\Big|_{r_b=r_{b,outer}} = -H_{b_{ext}} \left(T_b\Big|_{r_b=r_{b,outer}} - T_{amb} \right) \quad (8)$$

where $H_{b_{ext}}$ is the convection heat transfer coefficient of the bush to the outside medium.

- Heat exchange conditions at the interfaces of the bush and groove zones are taken into account by the following equations:

$$K_b \frac{\partial T_b}{\partial x}|_{x=x_{in}} = H_{b_{groove}} \left(T_b\Big|_{x=x_{in}} - T_{groove} \right) \quad (9)$$

$$K_b \frac{\partial T_b}{\partial x}|_{x=x_{out}} = -H_{b_{groove}} \left(T_b\Big|_{x=x_{out}} - T_{groove} \right) \quad (10)$$

where $H_{b_{groove}}$ is the convection heat transfer coefficient of the bush to the fluid.

2.3. Numerical Procedure

The equations in Section 2.1 are written in a discretized form using the finite volume method and solved iteratively by the vectorized Stone's strongly implicit procedure [9]. The programming language used is Fortran; Figure 1 shows the flowchart of the THD numerical program. The convergence criteria are chosen as follows: convergence on the pressure and temperature fields is obtained when the maximum relative difference is less than 10^{-6} or 10^{-5}, respectively; and convergence of the numerical process is achieved when the relative errors on the load are less than 10^{-5} on the magnitude and less than 10^{-4} on the attitude angle.

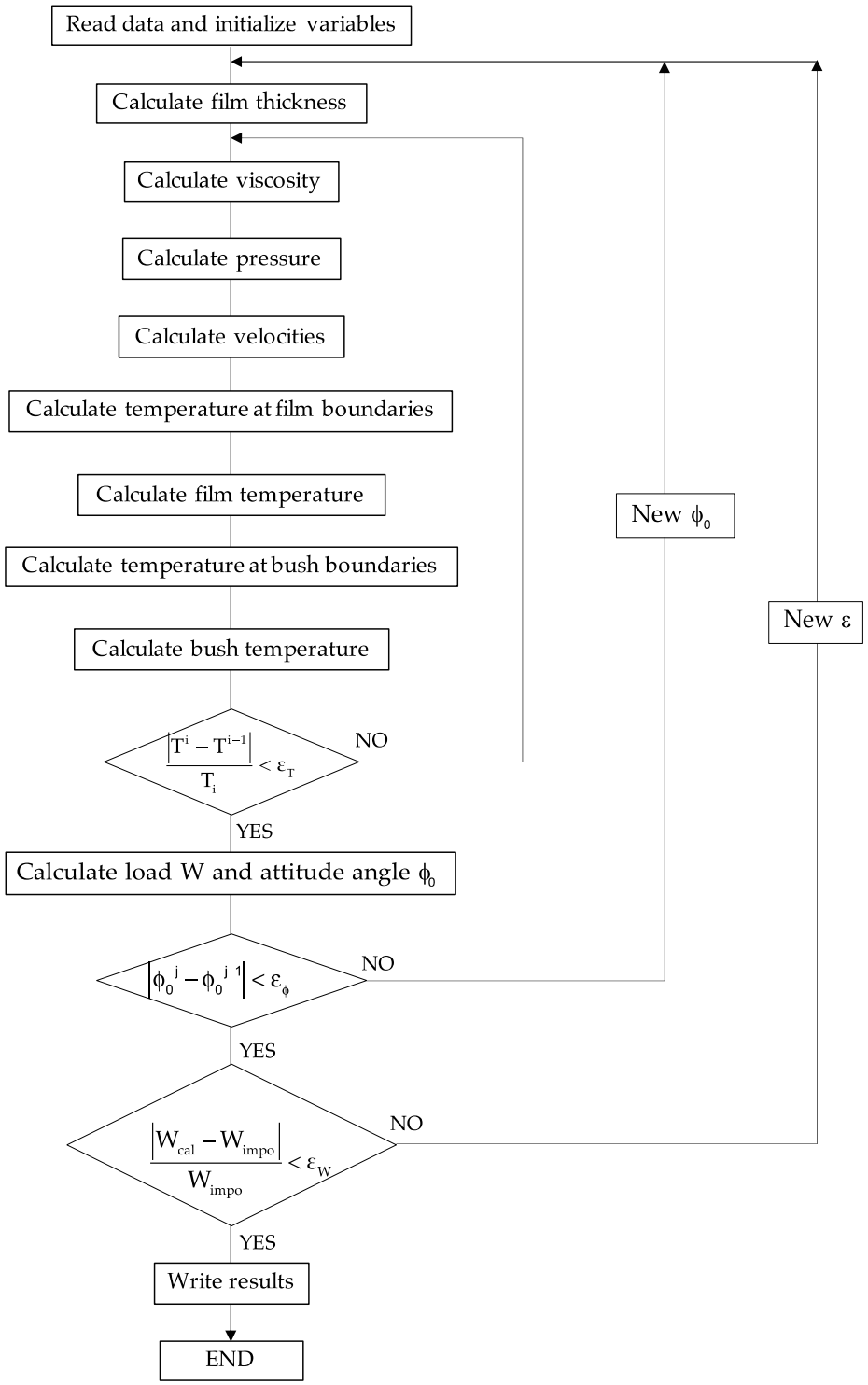

Figure 1. Flowchart of the THD numerical program.

3. Validation with Scientific Literature

To validate the numerical program, comparisons with the scientific literature are performed. In this study, comparisons with the study of Boncompain et al. [10] for a plain journal bearing and the study of Lund et al. [11] for a two-lobe journal bearing are performed. These bearings have no preload and no scratches. These simple configurations are chosen because of their simplicity. In addition, these simple tests may be useful as initial steps before simulating more, possibly complex, configurations with preloaded and

scratched journal bearings where the oil film geometry is more complex. Our simulations are performed using our THD model, with a recirculating coefficient $\alpha = 0.85$. The operating conditions and the geometrical characteristics of the bearings can be found in the relevant authors' articles.

3.1. Comparison with Boncompain et al.'s Numerical and Experimental Results

Figure 2 shows comparisons of the fluid pressure and temperature in the mid-plane of the inner bush surface with the results obtained by Boncompain et al. (both their THD simulation and their experimental results). While the THD model of the Boncompain et al. uses the finite difference method, our THD model uses the finite volume method. Input parameters and other assumptions are kept the same. The results show a good agreement between the two THD simulations for pressure. The discrepancy in the pressure gradient is tiny, and the maximum pressures are almost the same (only a minor difference in the locations of the maximum pressures can be observed). For the temperature profiles, the discrepancies are greater, the difference in the full oil film being about 2 K and in the cavitation zone about 5 K. Our simulation results are lower than those of Boncompain et al., who explained the minor discrepancy in the ruptured film zone by the fact that the deformations were not taken into account. It can be noted that our simulation is much closer to the experimental data in the rupture zone, and that the differences in the active zone are less than 1 K. Overall, the results obtained are satisfying in terms of tendency and accuracy for both pressure and temperature.

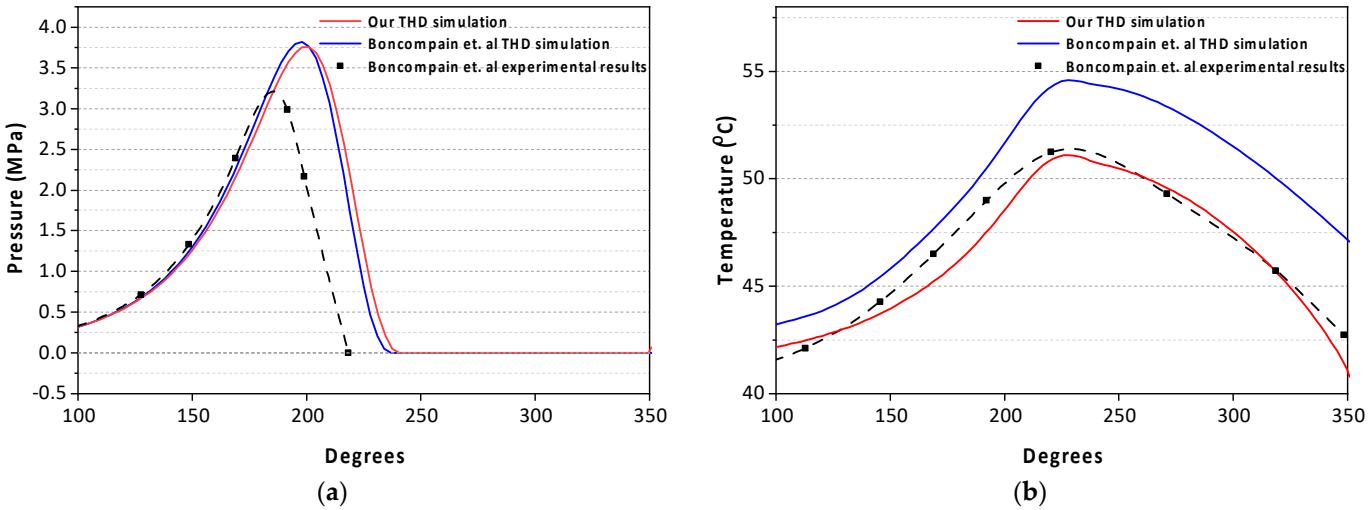

Figure 2. Comparisons between our simulations and Boncompain et al.'s results for a journal bearing with an eccentricity ratio of 0.8 and a rotational speed of 2000 rpm for (**a**) pressure and (**b**) temperature in the bearing mid-plane.

3.2. Comparison with Lund et al.'s Numerical and Experimental Results

Figure 3 shows comparisons of the fluid pressures in the mid-plane of the internal bush surface with the results obtained by Lund et al. (both their THD simulation and their experimental results), with an applied load of 8600 N and a rotational speed of 3500 rpm. The results show very good agreement between the THD simulations. The simulation results show minor discrepancies when compared to the experimental data, and again this is certainly because the thermal deformations of the solid surrounding parts were not considered in these models.

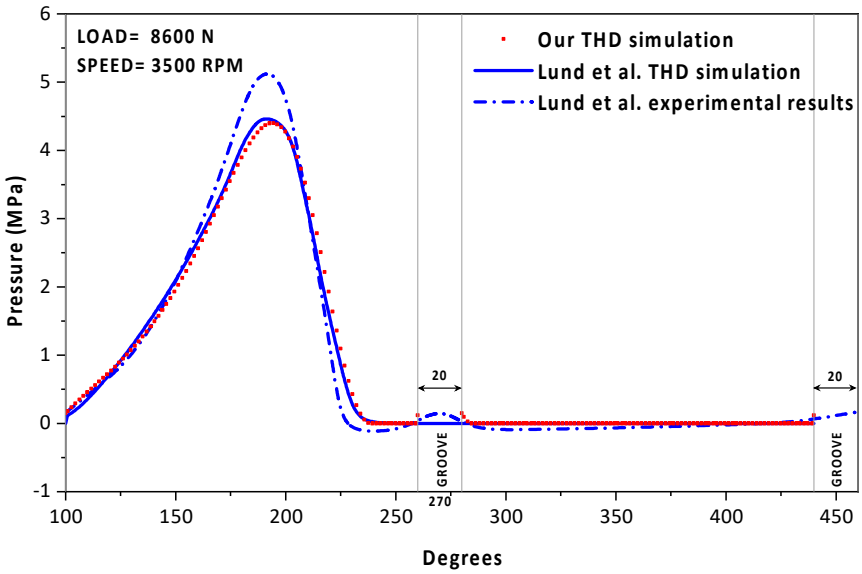

Figure 3. Comparisons of pressure profiles in the bearing mid-plane between our numerical results and Lund et al.'s results, for a two-lobe journal bearing with an applied load of 8600 N and a rotational speed of 3500 rpm.

Figure 4 compares the temperature profiles at the film/bush interface in the bearing mid-plane, with an applied load of 5600 N and a rotational speed of 3500 rpm. The results also show good agreement between the simulations in the full-film zone, but larger discrepancies in the film rupture zone. When compared to the experimental data, large discrepancies are observed in the cavitation zone for all the simulations. Our simulation results in the film rupture zone lie between Lund et al.'s simulation results and the experimental data, and are a little closer to the experimental results than are Lund et al.'s results. In general, our simulation results are in good agreement with Lund et al.'s simulations and the experimental data.

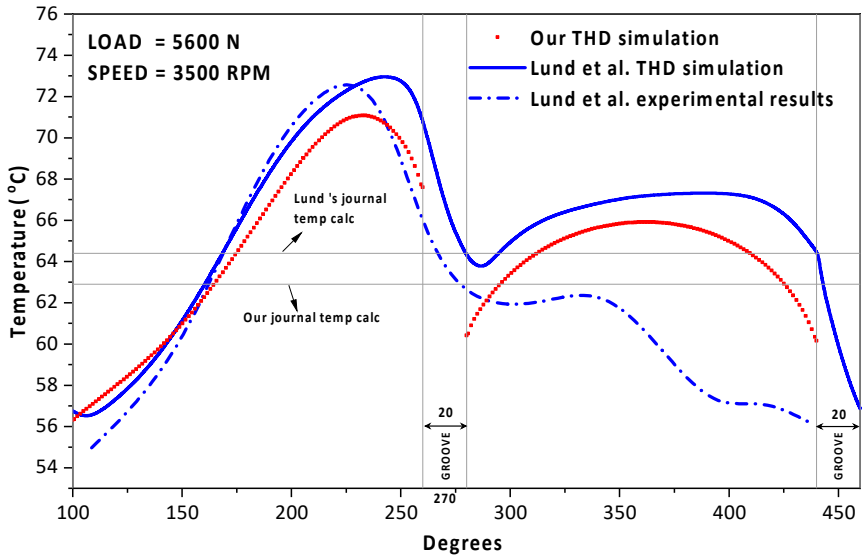

Figure 4. Comparisons of the film/bush interface temperatures in the bearing mid-plane between our numerical results and Lund et al.'s results, for a two-lobe journal bearing with an applied load of 5600 N and a rotational speed of 3500 rpm.

4. Comparison with Experimental Data

4.1. Experimental Setup

The experiments were carried out using the journal bearing test rig at the Pprime Institute presented in [5]. This test rig has been used successfully for numerous experiments for journal bearings over the past forty years. The maximum rotational speed of the shaft in this test rig is about 10,000 rpm and the maximum load-carrying capacity is 10,000 N. A torque meter allows us to measure the friction torque induced by hydrodynamic forces in the fluid film. A hydraulic system is used to control both the feeding pressure and feeding temperature so that they are constant in all tests.

Several experiments were conducted, particularly with a two-lobe journal bearing with a preload of 0.524, for three bearing configurations: no scratch, one scratch, and two scratches with varying axial locations. The major parameters of the scratches which were created at the surface of the journal are the following: 2 mm in width, and scratch depth of 260 µm for the one-scratch bearing and 116 µm for the two-scratch bearing; the locations of the scratch were at L/2 for the one-scratch bearing, and at L/3 and 2L/3 for the two-scratch bearing. Details on the bearing geometry, operating conditions, and other information can be found in [3]. The simulations were performed with an applied load of 6000 N and a rotational speed of 3500 rpm. Table 1 presents the data used for the simulations.

Table 1. Data for simulations.

Bearing and Lubricant Properties			**Unit**
Journal diameter	d	99.908	mm
Bearing diameter	D	100.058	mm
Bearing length	L	68.4	mm
Angular amplitude of each lobe	β	145	deg
Preload ratio	a	0.524	mm
Horizontal radial clearance	C	143	µm
Vertical radial clearance	C_b	68	µm
Radial thickness of bushing	R_b	20	mm
Lubricant		ISO VG 46	
Viscosity at 40 °C	μ_{40}	0.0416	Pa.s
Viscosity at 60 °C	μ_{60}	0.0191	Pa.s
Lubricant density	ρ	850	kg/m^3
Specific heat	C_p	2000	J/kg.K
Thermal conductivity	K_f	0.13	W/m.K
Supply pressure	P_{sup}	0.17	MPa
Supply temperature	T_{sup}	43	°C
Recirculating coefficient	α	60% and 100%	

4.2. Validation for Bearing with No Scratch

The first comparison with the experimental data is for a configuration of a non-scratched bearing under an applied load of 6000 N and a rotational speed of 3500 rpm.

Figure 5a shows the comparison between the simulation and the experimental results for the pressure profile in the bearing mid-plane. The agreement is very good in terms of shape and value, with a maximum difference of about 5.4%. The maximum pressures are at the same location, and the locations of the ruptured film positions are almost the same, as well. Figure 5b compares the results for the temperature profiles at the film/bush interface, again in the bearing mid-plane. There are minor discrepancies on a point-to-point basis, but the trend is in good agreement. The discrepancy is larger in the loaded lobe, with a maximum value of about 4 K compared to only about 2 K in the unloaded lobe. The temperatures calculated for the loaded lobe tend to be lower than the measured data. In contrast to this, in the unloaded lobe very good agreement is observed. There are several possible explanations for these results. One possibility is that the model does not take into account the mechanical and thermal deformations, which have a strong influence on the bearing performance, and the deformations produce more intensive effects on the loaded

lobe than on the unloaded load [12–14]. Another possible reason arises from the boundary condition at the outer surface of the lobes. The entire outer surface of the unloaded lobe has no direct contact with other surfaces, and the thermal boundary in this zone is a heat convection to the ambient medium. On the other hand, the loaded lobe has direct contact with the housing support in a portion of the outer surface of this lobe (about 40%, for an angular coordinate between 150° and 210°); in this region, the outer surface of the bearing support is one of the components of the hydrostatic bearing employed for applying the external radial load to the bearing. The heat exchange in this zone should thus be treated differently, as shown by Kucinschi et al. in [15]. However, it is difficult to model the heat exchange between the bearing and the supporting system completely, and this is unfortunately not yet included in our model.

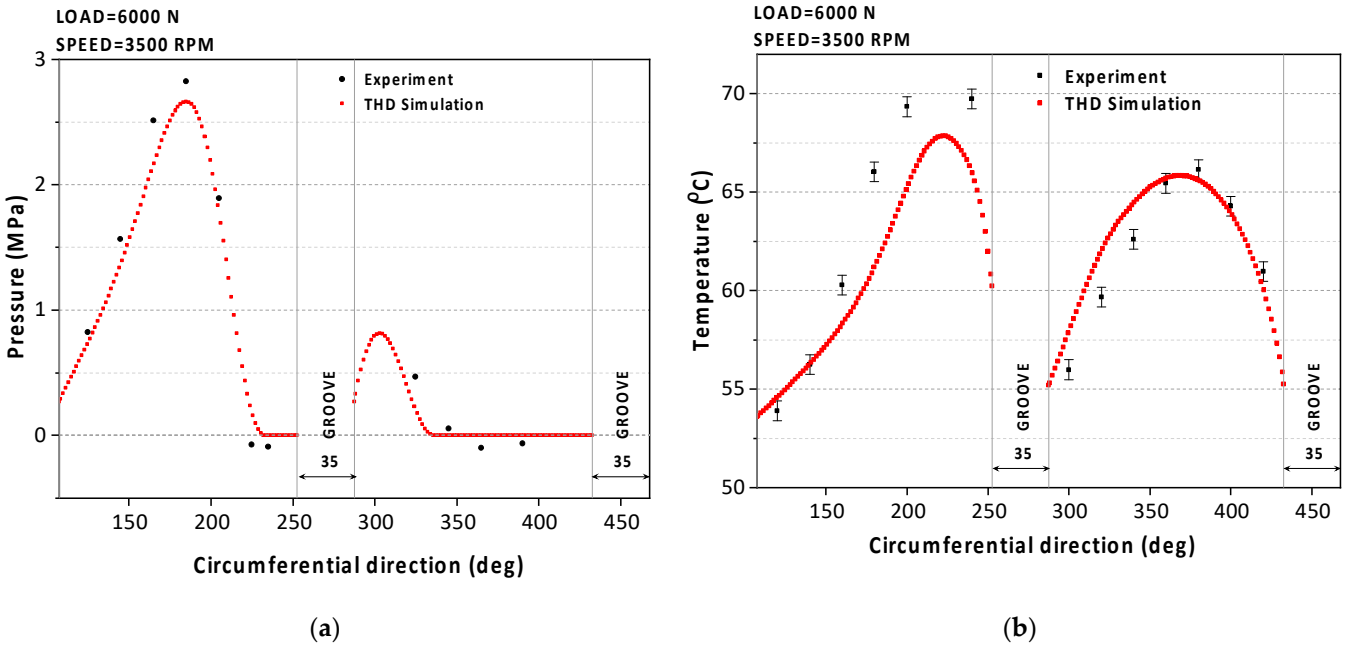

Figure 5. Simulation versus experiment in the bearing mid-plane for (**a**) pressure and (**b**) film/bush interface temperature.

Figure 6 compares the essential global parameters of the bearing: maximum pressure, maximum temperature in the bearing mid-plane, friction torque measured in the inner surface of the bush, and axial oil flow rate. The differences are about 5.94% and 2.73% for the maximum pressure and maximum temperature, respectively. The difference for the friction torque is about 3.57%, and it is only 0.09% for the oil flow rate. Overall, all the results obtained by the simulations are in very good agreement with the experimental data.

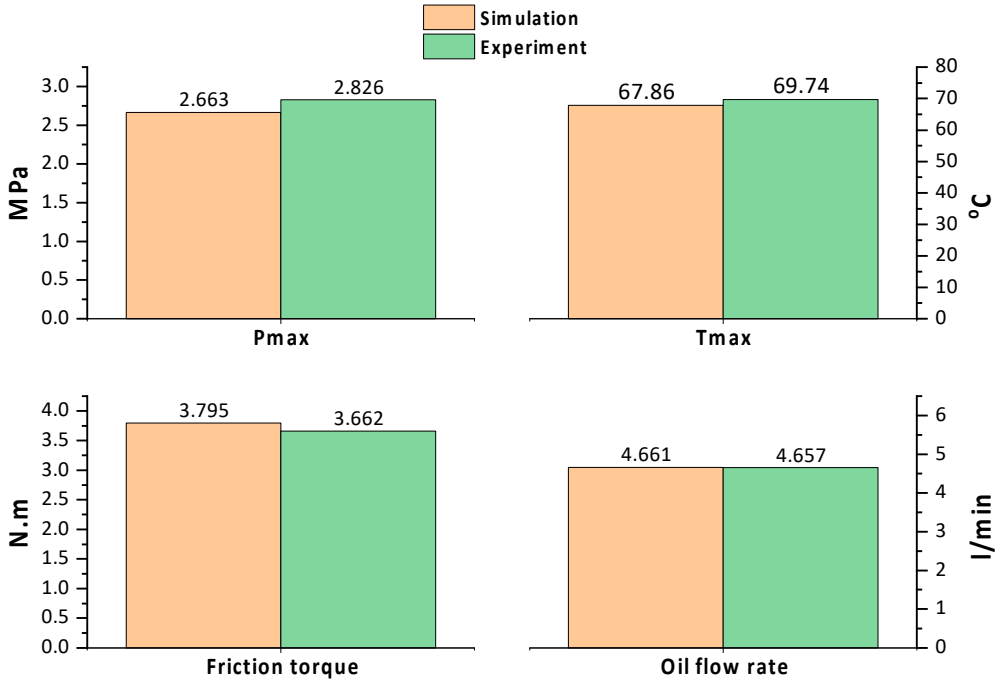

Figure 6. Simulation versus experimental data for P_{max}, T_{max}, friction torque, and axial oil flow rate.

4.3. Validation for a Bearing with One Scratch

The second comparison was performed for a scratched bearing with one scratch located in the bearing mid-plane. To observe the greatest influence on the bearing performance of the thermal effects and high eccentricity due to the presence of the scratch, we only present here a comparison for the high speed and high load case with a deep scratch. The operating conditions are 6000 N for the applied load and 3500 rpm for the rotational speed. The scratch depth and width are 260 µm and 2 mm, respectively. Two simulations were performed under isothermal and THD regimes to compare with the experimental data. For the isothermal regime, the average constant temperature was estimated to be equal to 65 °C.

Figure 7a–c present, respectively, the surfaces of the oil film thickness, the pressure, and the film/bush interface temperature of the bearing. It can be seen in Figure 7a that there are large gradients in the film thickness in the axial direction in the scratch region. At the circumferential location of the minimum film thickness, the film thickness is about 31 µm, while it is obviously about ten times higher, about 291 µm, in the scratch zone. It is therefore possible to observe a substantial drop in the pressure in this region. As expected, the pressure in the scratch region drops significantly and the pressure profile is strongly modified (Figure 7b). The pressure drops lead to a modification in the temperature profile that is less significant than the modification in the pressure profile—it decreases slightly in the scratch zone (Figure 7c).

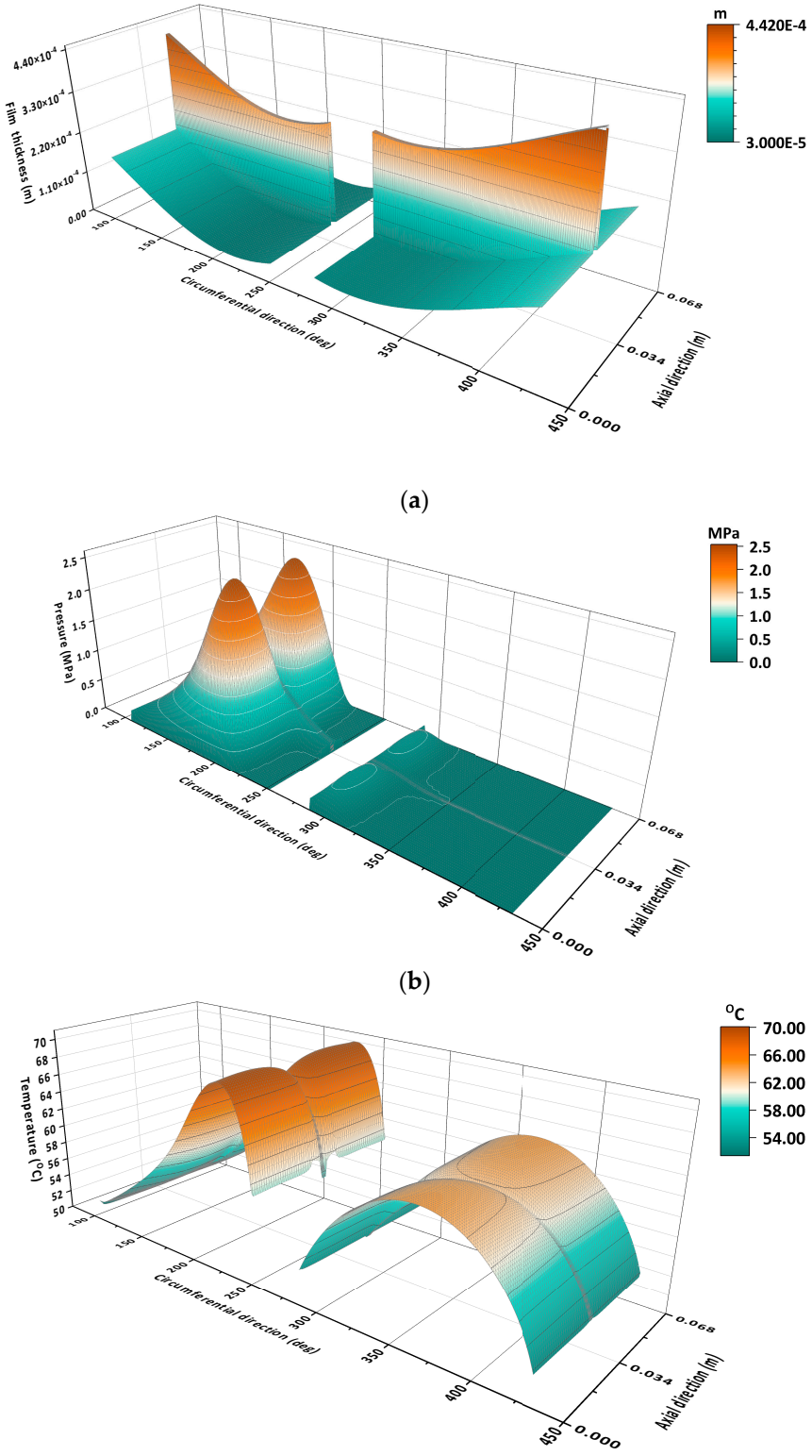

Figure 7. Three-dimensional profiles for a one-scratch journal bearing of (**a**) film thickness, (**b**) pressure, and (**c**) film/bush interface temperature (6000 N; 3500 rpm).

Figure 8 shows the results obtained in the bearing mid-plane. Figure 8a compares the pressure profiles and the experimental data. It can be seen that the THD model predicts the pressures, in terms of both the value and the profile, quite accurately. It

also results in greater accuracy than the global isothermal model, as expected. For the temperature comparison shown in Figure 8b, the THD solution and the experimental data are in good agreement in terms of the tendency. However, on a point-to-point basis, minor discrepancies are observed. The discrepancy is larger in the loaded lobe than in the unloaded lobe, as the maximum temperature difference in the loaded lobe is about 5 K while in the unloaded lobe it is only 2 K. This tendency seems to be consistent, as it was also obtained for the non-scratch bearing.

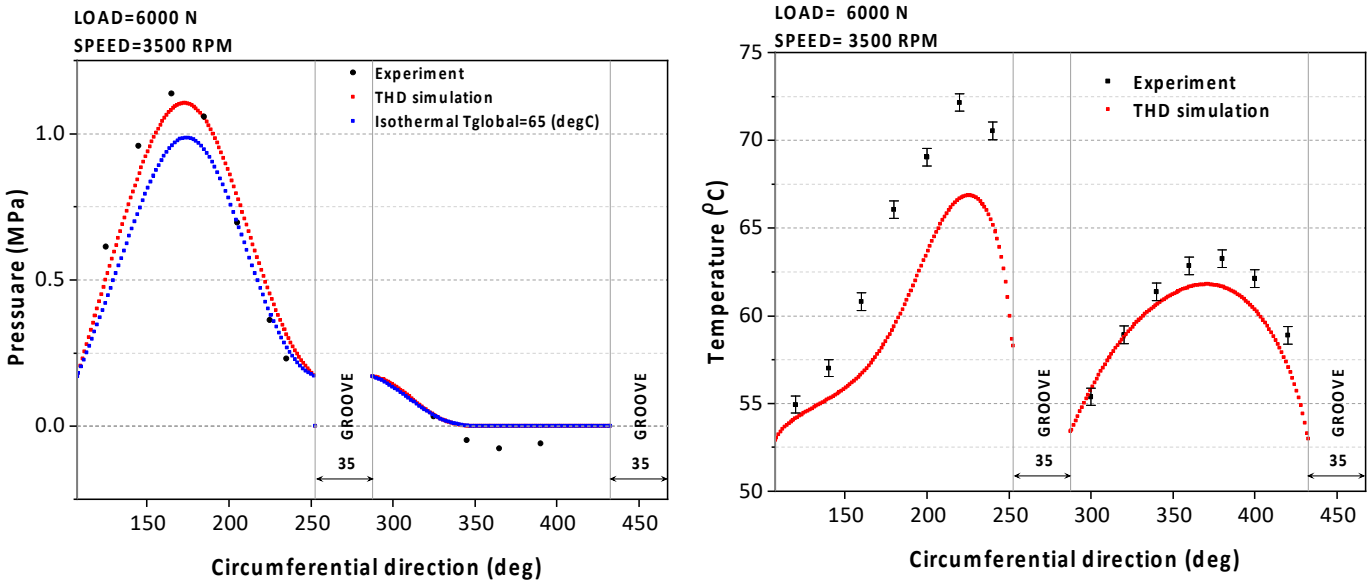

Figure 8. Simulations versus experiment in the bearing mid-plane of a one-scratch journal bearing (**a**) pressure and (**b**) film/bush interface temperature.

Table 2 shows a comparison between the calculated values and the experimental data for several global bearing performance parameters. It can be seen that in the bearing mid-plane, the difference between the maximum pressures is very good, at only 3.34%, while it is higher for the maximum oil temperatures, at 7.62%. For the friction torque measured on the inner surface of the bush and the volume flow rate, the differences are higher, at 11.44% and 13.62%, respectively.

Table 2. Comparison of global parameters for the one-scratch bearing (6000 N; 3500 rpm).

Parameters	Experiment	Simulation	Percentage Difference
Maximum pressure (MPa)	1.14	1.10	3.34%
Maximum oil temperature (°C)	72.16	66.86	7.62%
Friction torque (N.m)	3.71	4.16	11.44%
Flow rate (l/min)	3.97	4.55	13.62%

4.4. Validation for a Bearing with Two Scratches

The third comparison with the experimental data was performed for a scratched bearing with two scratches located in the axial positions L/3 and 2L/3. The operating conditions were the same as in the previous paragraph: 6000 N for applied load and 3500 rpm for rotational speed.

It was observed in the previous section that the scratch significantly modifies the pressure profile as well as the temperature field. The presence of scratches could therefore induce a substantial loss in the load capacity of the bearing. For this reason, and for a given operating condition of the bearing, it is helpful to find a rough estimate of the maximum value of the scratch depth for which the bearing can create sufficient hydrodynamic pressure, using Reynolds' solution, to support the applied load and rotational speed. It is observed in our simulations that, under a certain operating condition of the bearing, the THD model cannot converge to a final solution if the scratch depth is greater than a limiting value. Therefore, to obtain a good estimation of the limit of the scratch depth that can be simulated under the THD regime, we performed simulations under isothermal regimes for global temperatures of 45 °C and 65 °C before simulating the bearing under the THD regime. These isothermal simulations do not usually take much computing time to converge, when compared to the THD simulations. The results obtained are presented in Figure 9a,b for the cases of a global temperature of 45 °C and 65 °C, respectively. It can again be seen that scratches induce strong effects on bearing performance. Increasing the scratch depth increases the eccentricity and decreases the minimum film thickness, because the pressure drops in the scratch zone. Therefore, in order to support the same applied load, the bearing must operate under a higher eccentricity, corresponding to a lower minimum film thickness. Thermal effects also play an important role in the performance of the scratched bearing. In the model with a low global temperature of 45 °C, and with scratch depths of up to 341 μm, the model can converge to a solution. However, in the case of a higher global temperature of 65 °C, the model could not converge to a solution with scratch depths greater than 181 μm, because the minimum film thickness converged to zero. This could be explained by the fact that, when the scratch depth reaches the critical values (e.g., 341 and 181 μm), transition to turbulence of the flow can occur in the scratch region because the Reynolds number can reach a critical value. Therefore, it invalidates the generalized Reynolds equation in this zone, leading the model to fail to converge to a final solution. The Reynolds number for the bearing is directly proportional to the film thickness and inversely proportional to the fluid viscosity. Therefore, with the higher global temperature (lower fluid viscosity), the lower admissible scratch depth (lower film thickness) obtained seems reasonable.

These limit values of scratch depths are different depending on the operation conditions for the bearing (i.e., load and speed) and also on the thermal conditions. With the THD model, this value can even be lower because the calculated temperature may be higher, corresponding to higher thermal effects. This analysis is helpful since it gives initial estimates for the maximum admissible scratch depth and bearing position (eccentricity and attitude angle) for each scratch depth, which are useful inputs for THD simulations.

To visualize the modification of the pressure profiles under the effects of different scratch depths, simulation results obtained from the isothermal model with a global temperature of 65 °C were plotted in Figure 10. The pressure in the circumferential direction in the bearing mid-plane is shown Figure 10a, while the pressure in the axial direction at the maximum pressure section is shown in Figure 10b. As can be seen in these figures, the pressure profiles are modified more significantly in the axial direction than in the circumferential direction. The pressure gradients in the circumferential direction are barely changed, while they are modified significantly in the axial direction because of the presence of the scratches in this direction. Recalling Figure 9, it is interesting to observe that the maximum pressure decreases with an increase in the scratch depth until a certain value, above which it starts to increase. The dominant pressure modification in the axial direction is the reason for this. However, it should be noted that pressure profiles can be different for other configurations with different numbers of scratches, scratch locations, and also operating conditions.

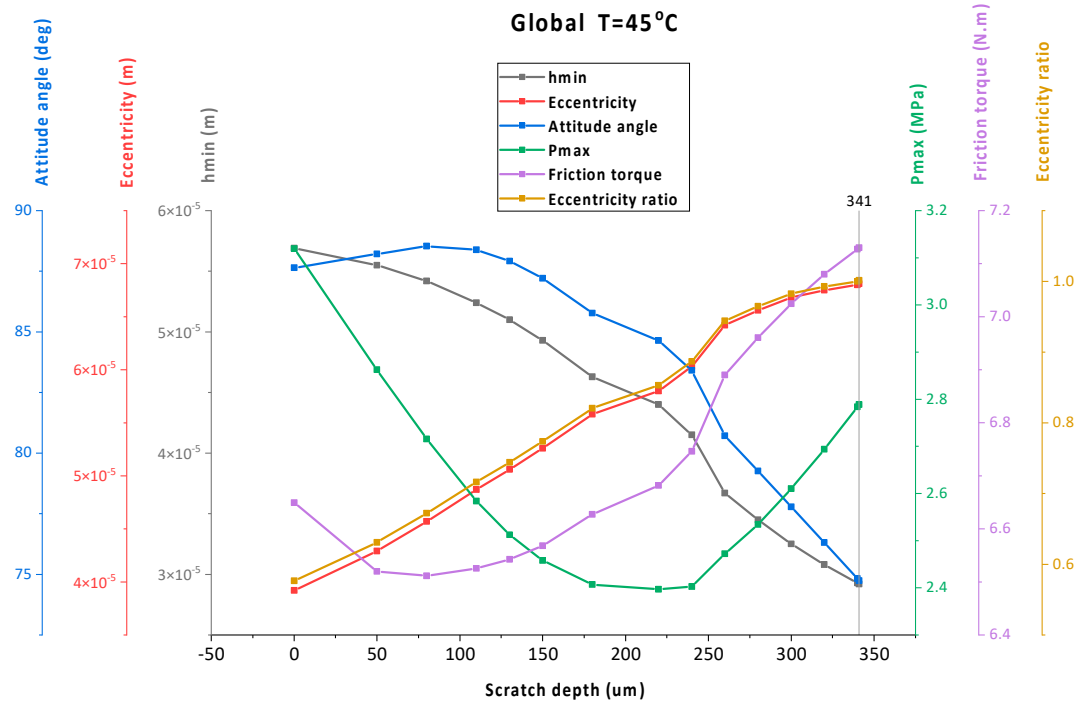

(**a**)

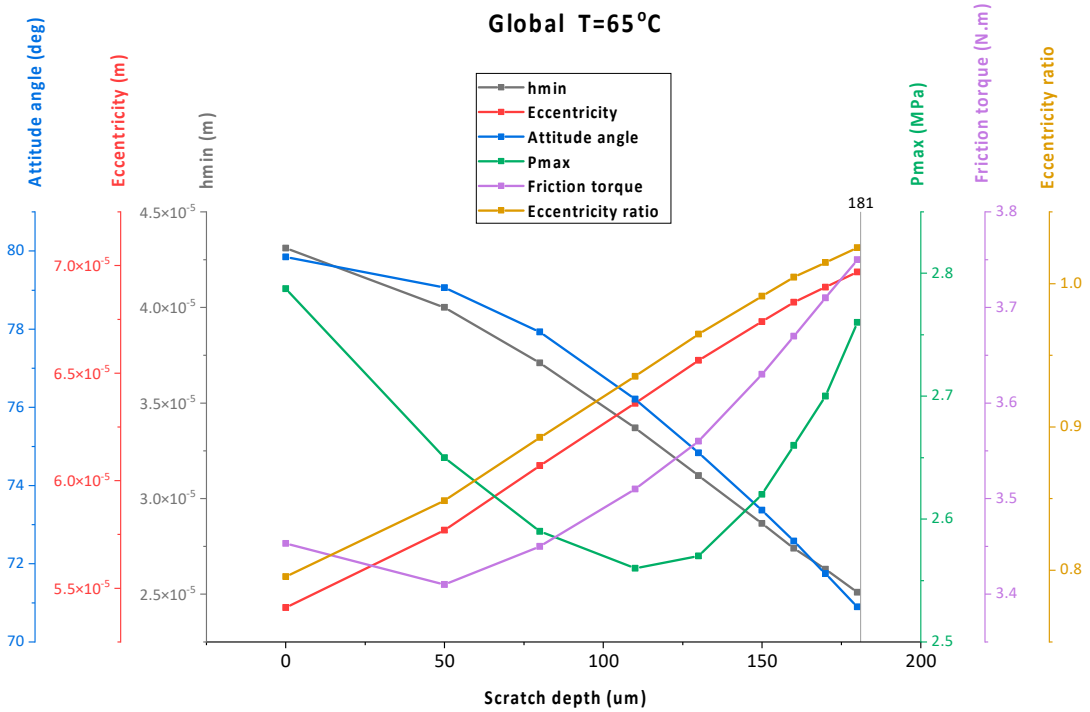

(**b**)

Figure 9. Effect of scratch depth on global bearing parameters under global isothermal regimes: (**a**) global temperature of 45 °C, (**b**) global temperature of 65 °C.

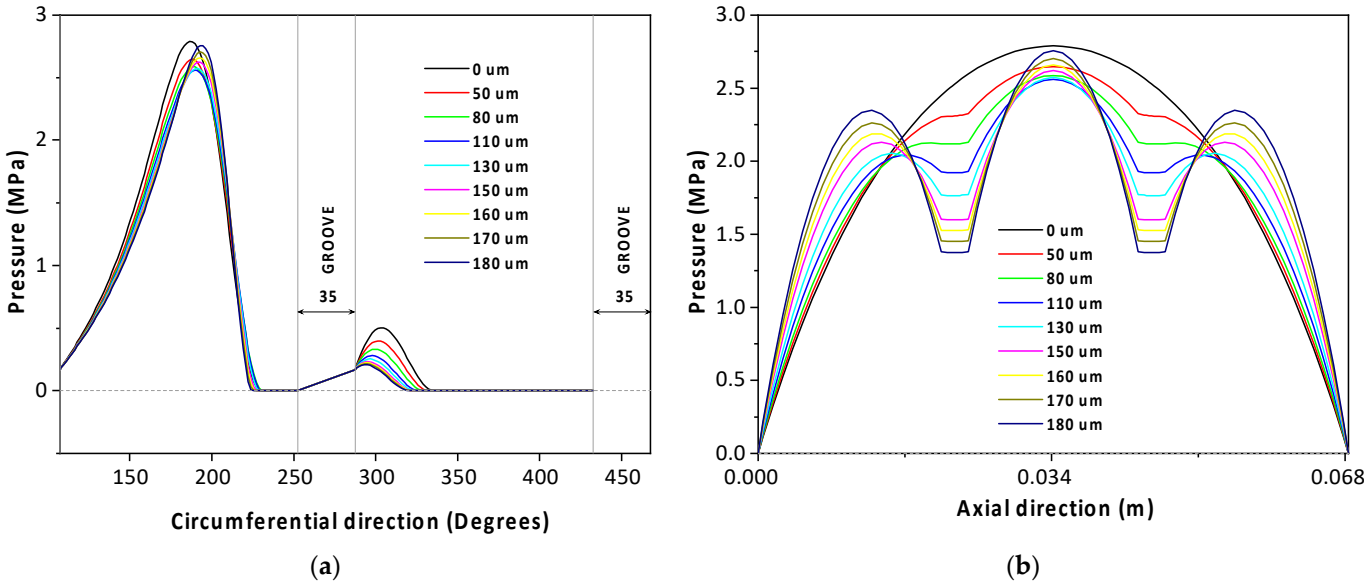

Figure 10. Pressure profiles for several scratch depths (**a**) in circumferential direction in bearing mid-plane and (**b**) in axial direction at the maximum pressure section.

To test the validity of the THD model when applied to two-scratch journal bearings, the third comparison with experimental data was performed. The same operating conditions were applied again. The scratch depth and width are 116 µm and 2 mm, respectively. The value of the scratch depth chosen is the highest experimental value available for the selected operating conditions.

Figure 11 presents the three-dimensional profiles of the oil film thickness (Figure 11a), pressure (Figure 11b), and temperature (Figure 11c) of the bearing. The same tendencies as for the one-scratch bearing can be observed, with the pressure and temperature dropping in the scratch zones and increasing in the remaining zones. Figure 12a compares the pressure profiles between the global isothermal simulation, the THD simulation, and the experimental data. It can be seen that the THD model predicts the pressures quite accurately in terms of both the value and the trend. As expected, it also results in a more accurate solution than the global isothermal solution. For the temperature comparison shown in Figure 12b, the THD solution and the experimental data are in good agreement in terms of the tendency. However, again, on a point-to-point basis, some discrepancies are observed. The discrepancy is larger for the highly loaded lobe than for the unloaded lobe, as the maximum temperature difference in the loaded lobe is about 7 K while that in the unloaded lobe is only 2 K. This tendency seems to be consistent with what was obtained for the non-scratch and one-scratch bearings. It could be the result of the limitations of the present model, which does not take into account the deformations and specific heat exchange conditions related to the test rig used for the experiments.

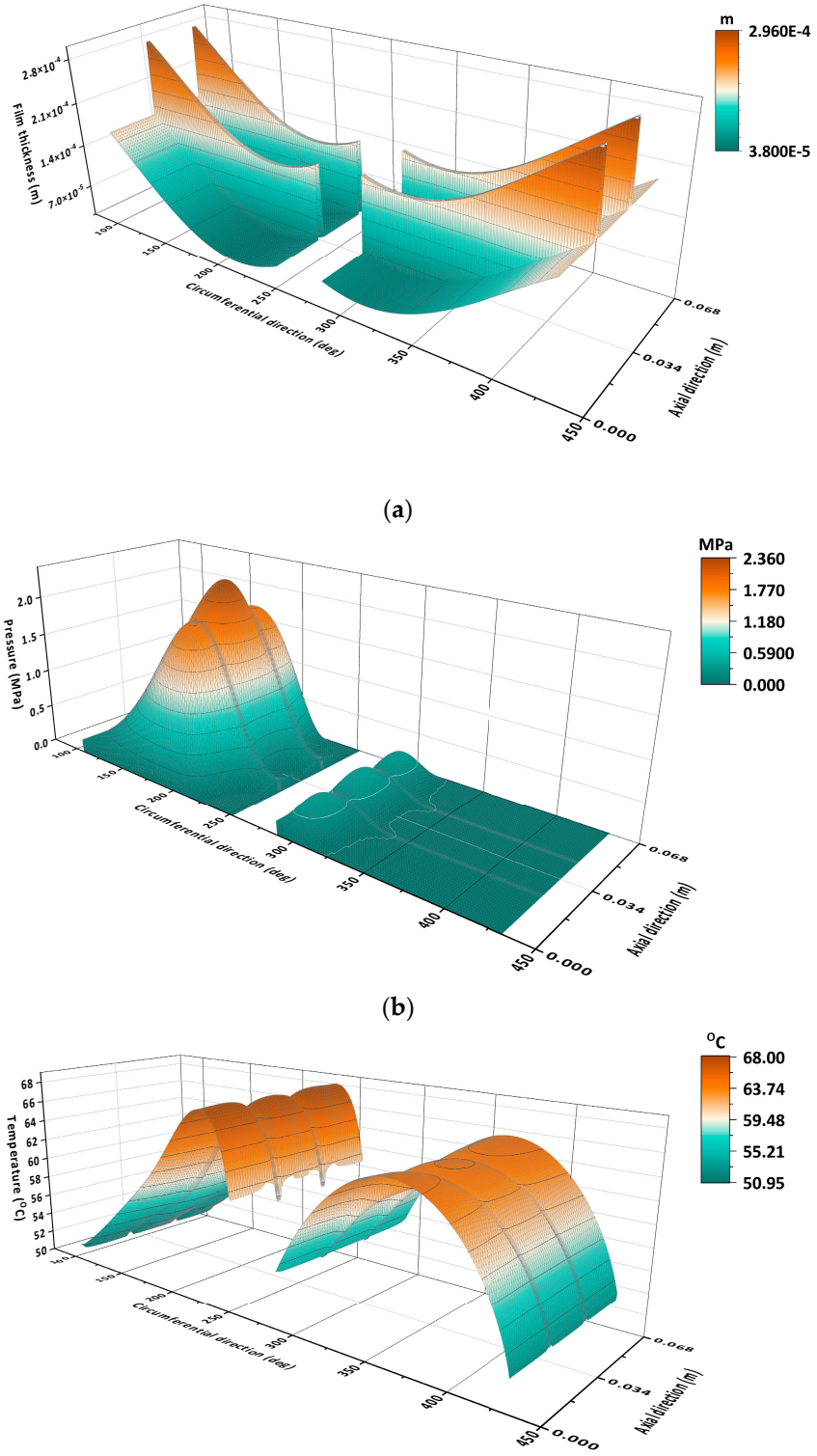

Figure 11. Three-dimensional profiles for a two-scratch journal bearing (**a**) film thickness, (**b**) pressure, and (**c**) temperature.

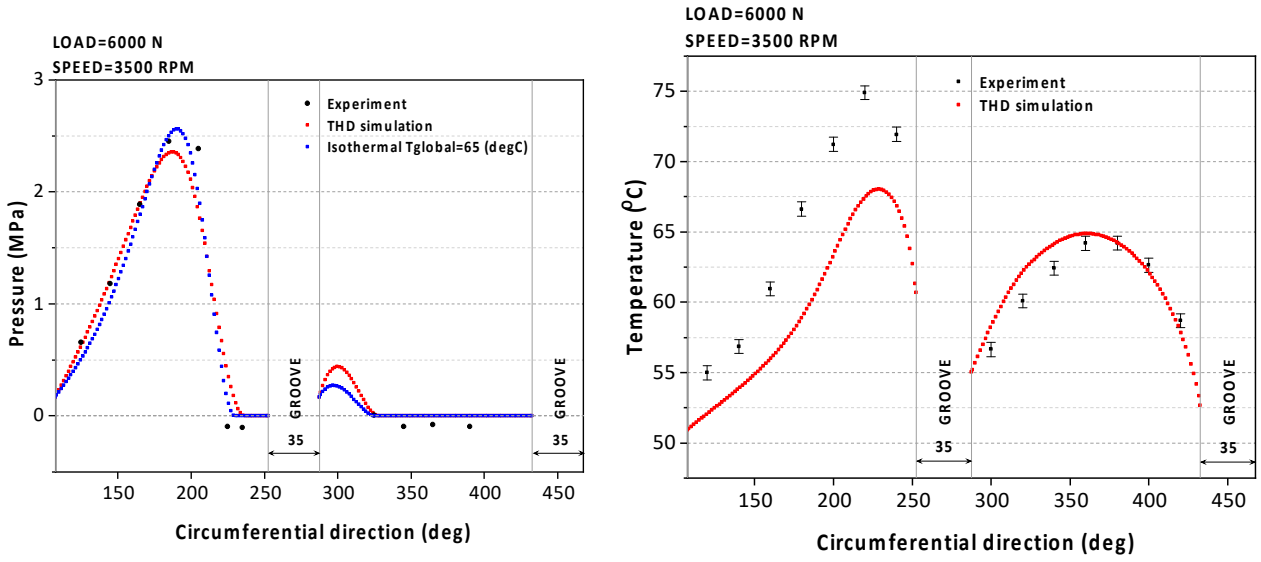

(**a**) (**b**)

Figure 12. Simulations versus experiment in the bearing mid-plane of a two-scratch journal bearing (**a**) pressure and (**b**) temperature.

Table 3 shows a comparison between the calculated and the experimental data for several global bearing performance parameters. It can be seen that in the bearing mid-plane, the difference between the maximum pressures is very good, at only 4.02%, while the difference is higher for the maximum oil temperatures, at 9.78%. For the friction torque measured on the inner surface of the bush and the volume flow rate, the differences are higher, at 5.39% and 10.58%, respectively.

Table 3. Comparison of global parameters for the two-scratch bearing.

Parameters	Experiment	Simulation	Percentage Difference
Maximum pressure (MPa)	2.36	2.45	4.02%
Maximum oil temperature (°C)	67.92	74.90	9.78%
Friction torque (N.m)	3.91	3.70	5.39%
Flow rate (l/min)	4.10	4.56	10.58%

5. Conclusions

To sum up, this study presents a numerical THD model that is able to simulate journal bearing behavior in the presence or absence of one or more scratches. The model was validated by comparing it with the scientific literature and also with experimental data. The model shows good agreement in pressure distribution and satisfactory agreement in temperature distribution and the global bearing performance parameters.

The initial numerical results confirm that presence of scratches induces a strong modification in the pressure profile in both shape and value, which is also observed in the experiments. It also changes the temperature profile, but to a less significant degree. Broader studies with different bearing conditions and scratch configurations will need to be performed to obtain a full understanding of the effects of scratches on the performance of scratched journal bearings. This type of analysis, and the associated simulations, for real applications will be very useful for bearing users in order to avoid any serious damage in turbomachinery and to determine the limits of operation of bearings with multiple scratches.

Furthermore, more accurate studies that take deformations and the heat exchange between the bush and bearing supporting system into account will need to be undertaken.

Author Contributions: Conceptualization, M.F. and J.B.; Formal analysis, A.T.V.; Methodology, A.T.V.; Software, A.T.V.; Supervision, M.F. and J.B.; Visualization, A.T.V.; Writing—original draft, A.T.V.; Writing—review & editing, M.F. and J.B. All authors have read and agreed to the published version of the manuscript.

Funding: This research received no external funding.

Institutional Review Board Statement: Not applicable.

Informed Consent Statement: Not applicable.

Data Availability Statement: Not applicable.

Acknowledgments: We gratefully acknowledge Yann Alexandre for his valuable experimental data used for comparisons in this study.

Conflicts of Interest: The authors declare no conflict of interest.

Nomenclature

L	Bearing length	m
h	Film thickness	m
p	Pressure	MPa
ρ	Lubricant density	kg/m^3
U	Shaft speed	rpm
x, y, z	Cartesian coordinates	
r_b, θ_b, z	Cylindrical coordinates	
x_{in}	Inlet circumferential coordinate	
x_{out}	Outlet circumferential coordinate	
μ	Dynamic viscosity	Pa.s
C_p	Lubricant specific heat	J/kg.K
u, v, w	Velocity components	rpm
T	Lubricant temperature	°C
T_b	Lobe temperature	°C
$r_{b,inner}$	Inner radius of the bush	m
$r_{b,outer}$	Outer radius of the bush	m
P_{sup}	Supply pressure	MPa
P_{amb}	Ambient pressure	MPa
T_{in}	Inlet temperature	°C
T_{out}	Outlet temperature	°C
T_{sup}	Supply temperature	°C
Q_{sup}	Supply flow rate	m^3/s
Q_{in}	Flow rate at the inlet	m^3/s
Q_{out}	Flow rate at the outlet	m^3/s
K_f	Thermal conductivity of the lubricant	W/m.K
K_b	Thermal conductivity of the bush	W/m.K
$H_{b_{ext}}$	Convection heat transfer coefficient of the bush outer surface	W/m^2.K
$H_{b_{groove}}$	Heat exchange coefficient of the groove wall	W/m^2.K

References

1. Branagan, L.A. Survey of Damage Investigation of Babbitted Industrial Bearings. *Lubricants* **2015**, *3*, 91–112. [CrossRef]
2. Dobrica, M.B.; Fillon, M. Performance Degradation in Scratched Journal Bearings. *Tribol. Int.* **2012**, *51*, 1–10. [CrossRef]
3. Giraudeau, C.; Bouyer, J.; Fillon, M.; Hélène, M.; Beaurain, J. Experimental Study of the Influence of Scratches on the Performance of a Two-Lobe Journal Bearing. *Tribol. Trans.* **2017**, *60*, 942–955. [CrossRef]
4. Bouyer, J.; Fillon, M.; Helene, M.; Beaurain, J.; Giraudeau, C. Behavior of a Two-Lobe Journal Bearing With a Scratched Shaft: Comparison Between Theory and Experiment. *J. Tribol.* **2018**, *141*. [CrossRef]
5. Bouyer, J.; Alexandre, Y.; Fillon, M. Experimental Investigation on the Influence of a Multi-Scratched Shaft on Hydrodynamic Journal Bearing Performance. *Tribol. Int.* **2021**, *153*, 106543. [CrossRef]

6. Bonneau, D.; Fatu, A.; Souchet, D. *Hydrodynamic Bearings*; ISTE: London, UK; John Wiley & Sons: New York, NY, USA, 2014; pp. 17–61. ISBN 978-1-84821-681-5.
7. Brito, F.P.; Miranda, A.S.; Claro, J.C.P.; Teixeira, J.C.; Costa, L.; Fillon, M. The Role of Lubricant Feeding Conditions on the Performance Improvement and Friction Reduction of Journal Bearings. *Tribol. Int.* **2014**, *72*, 65–82. [CrossRef]
8. Brito, F.; Miranda, A.; Claro, J.; Teixeira, J.; Costa, L.; Fillon, M. Thermohydrodynamic Modelling of Journal Bearings under Varying Load Angle and Negative Groove Flow Rate. *Proc. Inst. Mech. Eng. Part J J. Eng. Tribol.* **2014**, *228*, 955–973. [CrossRef]
9. Leister, H.-J.; Perić, M. Vectorized Strongly Implicit Solving Procedure for a Seven-diagonal Coefficient Matrix. *Int. J. Num. Meth. HFF* **1994**, *4*, 159–172. [CrossRef]
10. Boncompain, R.; Fillon, M.; Frêne, J. Analysis of Thermal Effects in Hydrodynamic Bearings. *J. Tribol.* **1986**, *108*, 219–224. [CrossRef]
11. Lund, J.W.; Tonnesen, J. An Approximate Analysis of the Temperature Conditions in a Journal Bearing. Part II: Application. *J. Tribol.* **1984**, *106*, 237–244. [CrossRef]
12. Bouyer, J.; Fillon, M. On the Significance of Thermal and Deformation Effects on a Plain Journal Bearing Subjected to Severe Operating Conditions. *J. Tribol.* **2004**, *126*, 819–822. [CrossRef]
13. Chatterton, S.; Dang, P.V.; Pennacchi, P.; De Luca, A.; Flumian, F. Experimental Evidence of a Two-Axial Groove Hydrodynamic Journal Bearing under Severe Operation Conditions. *Tribol. Int.* **2017**, *109*, 416–427. [CrossRef]
14. Dang, P.V.; Chatterton, S.; Pennacchi, P.; Vania, A. Effect of the Load Direction on Non-Nominal Five-Pad Tilting-Pad Journal Bearings. *Tribol. Int.* **2016**, *98*, 197–211. [CrossRef]
15. Kucinschi, B.-R.; Fillon, M.; Frêne, J.; Pascovici, M.D. A Transient Thermoelastohydrodynamic Study of Steadily Loaded Plain Journal Bearings Using Finite Element Method Analysis. *J. Tribol.* **1999**, *122*, 219–226. [CrossRef]